APPLICATIONS OF FINITE ELEMENT TECHNOLOGY TO REINFORCED CONCRETE EXPLOSIVES CONTAINMENT STRUCTURES

by

T. A. Shugar and T. J. Holland
Naval Civil Engineering Laboratory
Port Hueneme, CA 93043

and

L. J. Malvar
University of California, Davis
Davis, CA 95616

Paper Submitted to

Department of Defense Explosives Safety Board
Twenty-Fifth Explosives Safety Seminar

Anaheim, California
18-20 August 1992

Report Documentation Page

Form Approved
OMB No. 0704-0188

1. REPORT DATE	2. REPORT TYPE	3. DATES COVERED
AUG 1992		**00-00-1992 to 00-00-1992**

4. TITLE AND SUBTITLE	5a. CONTRACT NUMBER
Applications of Finite Element Technology to Reinforced Concrete Explosives Containment Structures	5b. GRANT NUMBER
	5c. PROGRAM ELEMENT NUMBER
6. AUTHOR(S)	5d. PROJECT NUMBER
	5e. TASK NUMBER
	5f. WORK UNIT NUMBER
7. PERFORMING ORGANIZATION NAME(S) AND ADDRESS(ES) **Naval Civil Engineering Laboratory, ,Port Hueneme,CA,93043**	8. PERFORMING ORGANIZATION REPORT NUMBER
9. SPONSORING/MONITORING AGENCY NAME(S) AND ADDRESS(ES)	10. SPONSOR/MONITOR'S ACRONYM(S)
	11. SPONSOR/MONITOR'S REPORT NUMBER(S)

12. DISTRIBUTION/AVAILABILITY STATEMENT
Approved for public release; distribution unlimited

13. SUPPLEMENTARY NOTES
See also ADA261116, Volume IV. Minutes of the Twenty-Fifth Explosives Safety Seminar Held in Anaheim, CA on 18-20 August 1992.

14. ABSTRACT
see report

15. SUBJECT TERMS

16. SECURITY CLASSIFICATION OF:			17. LIMITATION OF ABSTRACT	18. NUMBER OF PAGES	19a. NAME OF RESPONSIBLE PERSON
a. REPORT **unclassified**	b. ABSTRACT **unclassified**	c. THIS PAGE **unclassified**	**Same as Report (SAR)**	**27**	

ABSTRACT

Two widely available general purpose computer programs for three-dimensional nonlinear dynamic finite element analysis were applied to three types of reinforced concrete structures of recent interest to Navy explosive safety: a novel cylindrical missile test cell concept, flat slabs with variable shear steel, and a soil-covered roof slab for a new high performance magazine concept. Results from codified single-degree-of-freedom (SDOF) methods for design of explosive safety structures were considered and compared with finite element technology. An overview of these baseline studies is presented.

A commercial implicit finite element program was used to analyze the cylindrical missile test cell. Three-dimensional model construction, nonlinear concrete material modeling, and dynamic response were emphasized. Support for embedded reinforcement modeling was found to be very useful in construction of the model so as to retain the inherent anisotropic behavior of the composite structure. Concrete material modeling capability was highly sophisticated, but problematical in application when substantial cracking accumulated in the dynamic response. Sufficient results were nonetheless obtained to demonstrate the value of computational structural dynamics technology in providing detailed understanding of the behavior of complex explosive safety designs.

An explicit finite element program was used to analyze the dynamic response of two flat slabs subjected to conventional blast pressure levels. Elasto-plastic models included in the material library were used to model the material behavior of concrete and steel. The rebar pattern was modeled via the discrete reinforcement method; no embeded modeling capability existed. Measured residual deflections from field tests were compared to calculations from both three-dimensional finite element models and codified SDOF methods. In these limited data, the codified SDOF method was prone to unconservative results, while the finite element method bracketed the measured residual displacements, and further, successfully calculated observed failure modes and the onset of buckling in the reinforcement.

The explicit finite element program was also applied in the analysis of the soil-covered roof slab design. In this case, the blast load pressures were an order magnitude higher, and the concrete material response included hydrodynamic behavior. The three-dimensional finite element model also included discrete reinforcement modeling and elasto-plastic behavior of the rebar. The dynamic response of the slab was calculated up to onset of a localized failure mode. This failure mode was consistent with initial field test observations of breach failure modes in scale models of slabs.

It is concluded that commercial or available general purpose finite element programs for nonlinear dynamic analysis of reinforced concrete structures merit wider recognition and application in analysis and design of explosive safety systems. However, these programs have definite strengths and weaknesses, and consequently proficiency in their application must be developed to exploit them as resources.

INTRODUCTION

Traditional design of reinforced concrete structures to resist blast loads has been based on structural dynamics of elastic-plastic lumped parameter models of one or two degrees of freedom. These models are well explicated in the classical reference by Biggs (1964). In addition to this analytical technology, design procedures are also based on field testing experience accumulated in explosive safety engineering for the past quarter century. The combination of traditional structural dynamics and field test experience has led to a semi-empirical method for the design of explosive safety facilities as embodied by the standard Tri-Services guide, NAVFAC P-397 Design Manual (1991). However, this guide does not address modern computer methods in structural dynamics and finite element methods. It neither promotes nor precludes their use in the analysis and design of explosive safety facilities. Nonetheless, it is of interest to investigate how well these modern methods perform, and whether they merit further recognition in conjunction with codified procedures in explosive safety.

Objective

The objective of this paper is to discuss the effectiveness of modern computational structural dynamics methods which have been applied to recent problems in naval explosive containment facilities constructed of reinforced concrete. The methods are embodied by two widely used general purpose, nonlinear dynamic, finite element computer programs. One is based on implicit and the other on explicit, temporal integration of the equations of motion. More detailed information on this subject is presented in a corresponding NCEL technical report (Shugar, et al., 1992).

Structural Analysis Models Studied

The reinforced concrete structures studied include a novel missile test cell concept subjected to an internal blast load, flat slabs subjected to close in blast loads and a soil-covered roof slab subjected to an internal blast load which has been recently proposed for a high performance magazine concept.

The unique feature of the missile test cell analysis is the complexity of the steel reinforcement model which was constructed using the embedded reinforcement model method. In contrast to this method discrete reinforcement models were employed for the analysis of the flat slabs and the soil-covered roof slab, both of which have comparatively regular patterns of reinforcement. The missile test cell analysis was addressed with the implicit code, ABAQUS (1989), whereas the flat slabs and soil-covered roof slab were analyzed with the explicit finite element program, DYNA3D (Hallquist and Whirley, 1989). In general, implicit codes are suitable to analyses dealing with slow, sluggish dynamic loads, while the explicit codes are suitable to highly transient dynamic loads. On the other hand, reinforced concrete modeling capability is more substantial in ABAQUS than in DYNA3D. This is because the former supports modeling of complex reinforcement patterns, and because the concrete model is more sophisticated; it includes strain softening and orthotropic cracking behavior, for example.

The DYNA3D analysis of the flat slabs was noteworthy because some experimental data was available and was used to compare computed and measured dynamic response. Two slabs were studied, one with substantial shear steel reinforcement, and the other with no shear steel reinforcement. Further, comparisons included computed dynamic response as calculated according to the NAVFAC P-397 Design Manual.

The unusual feature of the the soil-covered roof analysis was the magnitude of specified blast loads. These were an order of magnitude higher than in the missile test cell analysis. This necessitated an auxiliary study of DYNA3D material models available for concrete behavior in the hydrodynamic range, as well as in the shear deformation range. In addition to discussion of the dynamic response of the roof, an approach to computing fragment and debris distance is also discussed.

NONLINEAR DYNAMIC FINITE ELEMENT ANALYSIS OF REINFORCED CONCRETE MISSILE TEST CELL

In this baseline study we addressed the problem of analyzing a reinforced concrete missile test cell (MTC) structure subjected to an internal blast load. The study employed ABAQUS Version 4.8, which is a general purpose implicit finite element program for static and dynamic analysis. The study featured accurate replication of three-dimensional geometry and composite structural behavior for a complex reinforced concrete design. Accurate modeling of an entire reinforced concrete structure was pursued, and how current technology addresses nonlinear material behavior such as cracking and crushing of concrete was studied.

Though the study included linear static analyses, eigenvalue analyses and linear dynamic analyses of the MTC, these and other results are generally omitted for brevity. The discussion given emphasizes the MTC model development, the nonlinear concrete material model, and the numerical results for the nonlinear dynamic response of the MTC wall.

Missile Test Cell Model Development

Commercial computational methods that may be used for the analysis of a complex reinforced concrete missile test cell are limited to ones based on implicit temporal integration algorithms. This adversely impacts the requirement for computational efficiency. For large scale problems this may mean that the analysis will be prohibitive. Codes based on implicit temporal integration are technically capable of predicting high frequency response, and are capable of predicting both nonlinear material and nonlinear geometric behavior, but the required computational power can be prohibitive.

Blast Load and Expected Structural Response. To model the MTC so that its dynamic response can be accurately computed, the blast load should be determined as closely as possible. For purposes of this investigation, the MTC is presumed subjected to the two-phase design (internal) blast load graphed in Figure 1 which is based on an inadvertent detonation of a missile warhead.

The bilinear triangular pressure history shown is composed of an initial triangular shock pressure phase and a subsequent triangular gas pressure phase (Murtha and Dede,1988). In this case, the pressure is further assumed uniformly distributed over all internal surfaces of the MTC. The shock pressure history includes a 2,560-psi peak pressure with a duration of 1.75 milliseconds and a specific impulse of 2,240 psi-ms.

The calculation of the gas pressure phase is based on containment of the products of detonation. This phase has a comparatively low magnitude, long duration triangular pressure history. The semi-empirical method used and the computer program developed for calculating the gas pressure loads are described by Tancreto and Helseth (1984). According to this methodology, the gas pressure history depends on the shock pressure and various geometric and physical properties of any venting mechanisms present. In the case of the MTC, a frangible circular aperture in the back wall constitutes a venting mechanism which is factored into the computation. The resulting gas pressure history shown has a peak value of 307 psi, a duration of 177 milliseconds, and a specific impulse of 27,155 psi-ms which is substantially larger than the specific impulse of the shock phase.

MTC Configuration and Steel Reinforcement. The MTC is fundamentally a reinforced concrete thick-wall cylinder with thick circular plate endwalls. The walls of the structure are 32 inches thick, and the inside chamber is approximately 20 feet in diameter and 30 feet in length. Regarding model construction, these simple geometrical aspects are deceiving because the geometrical complexity of the steel reinforcement is substantial. Modeling this complexity represented the major challenge to the development of the finite element model of the MTC for it was desired to retain, as closely as possible, the anisotropic behavior inherent in its composite design.

Description of the MTC steel reinforcement design is facilitated by subdividing it into three sections as shown in Figure 2; they include the cylinder, the front wall and the back wall. The geometrical patterns shown in these graphics are the result of an intermediate stage of the reinforcement modeling procedure which employed computer aided design software. This stage was necessary to clarify and define the reinforcement patterns from data taken directly from design drawings of the MTC.

The hoop and longitudinal steel reinforcements for the cylinder subsection, which are indicated in Figure 2a, are comprised of #11 bars. Groups composed of four concentric hoop bars are located at stations every 6-inches along the length of the cylinder. To each of the four hoop bars there corresponds a layer of longitudinal reinforcement. Each layer contains 156 longitudinal bars equally spaced about the circumference at intervals of 2.3 degrees.

The reinforcement design for the back wall of the MTC is shown in Figure 2b. It is composed of two identical layers of mutually orthogonal hoop and radial bars. One layer each is embedded just beneath the inside and outside concrete surfaces of the wall.

The front wall reinforcement design shown in Figure 2c is more complex since the aperature is rectangular instead of circular to provide for a blast resistant access door. The radial steel is similar to the radial steel in the back wall in that only every other bar extends from the outer perimeter to the aperture. The radial reinforcement consists of 156 #6 bars, and the hoop bars are #11 bars in both end walls.

In addition to the primary reinforcement described, the MTC design also included shear steel and diagonal bars, which for clarity are omitted in these graphics. For example, the shear steel consists of stirrup bars tying together the four concentric layers of primary bars in the cylinder wall. These stirrup bars are meant to confine the concrete to the hoop and longitudinal steel bars. The diagonal bars are #11 bars, and they were intended to reinforce the interface between the cylinder and the front and back walls. To this end, a pair of crossing diagonal bars were included at each of 156 uniformly spaced stations around the two perimeter interfaces between the cylinder and end walls.

Three-Dimensional Finite Element Model. The three-dimensional finite element model of the MTC is shown in Figure 3. One plane of symmetry is exploited due to symmetry of the structure and applied load. Eight-node brick elements in which the displacement fields are interpolated linearly were prescribed. Two elements were prescribed through the thickness of the wall. Earlier models were also developed with four elements through the thickness, and linear static runs indicated that the radial stiffness of the MTC model was the same for either model. The model possessed 1300 nodes or 3900 degrees of freedom. PATRAN Plus (1989), Release 2.4, was employed to generate the basic three-dimensional models. It has ABAQUS file format translators for basic mesh and surface load information, but it does not support the ABAQUS embedded reinforcement data files which describe the reinforcement model.

Description of Embedded Element. The steel reinforcement model is constructed by the embedded reinforcement model approach. The advantage of this approach is that it provides a reasonably accurate replication of the effect of reinforcement while being convenient and expedient to implement into an existing finite element model. No changes to the aforementioned finite element model (Figure 3) were required to introduce the reinforcement model, in spite of the complexity of the reinforcement patterns. A recent discussion of the embedded reinforcement modeling method is provided by Cervera, Hinton and Hassan (1989).

A sketch of an embedded element is shown in Figure 4. This element is typical of the cylindrical wall of the MTC model, so that principal directions are labeled hoop, longitudinal and radial. Two such elements, each 16 inches thick, model the wall through its thickness. There are four layers of steel reinforcement in the wall, of which two exist within each element. Shown here is the inner element with the bottom node lying in the internal cylindrical surface of the wall, and the top node lying in the middle surface of the cylindrical wall. The exact locations of the two inner layers of reinforcement relative to the middle surface are indicated. Each layer is a smoothed composition of bars running through the element. Moreover, a layer possesses an anisotropic or directed stiffness corresponding to the percentage and direction of the steel. This stiffness is superimposed on the otherwise isotropic stiffness of the parent concrete element.

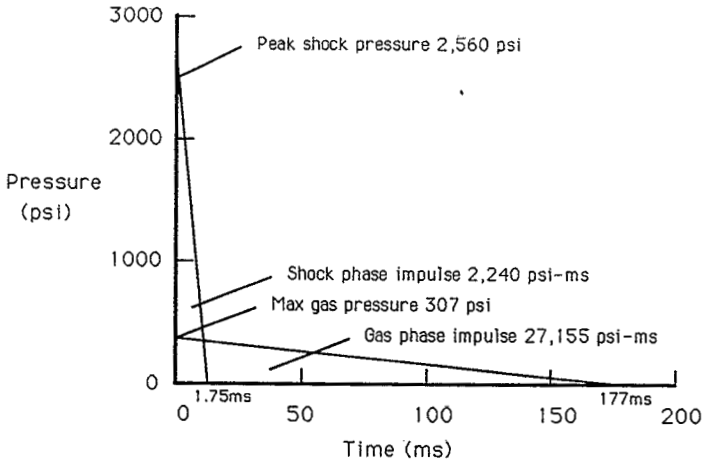

Figure 1. Assumed internal shock and gas pressure load for MTC.

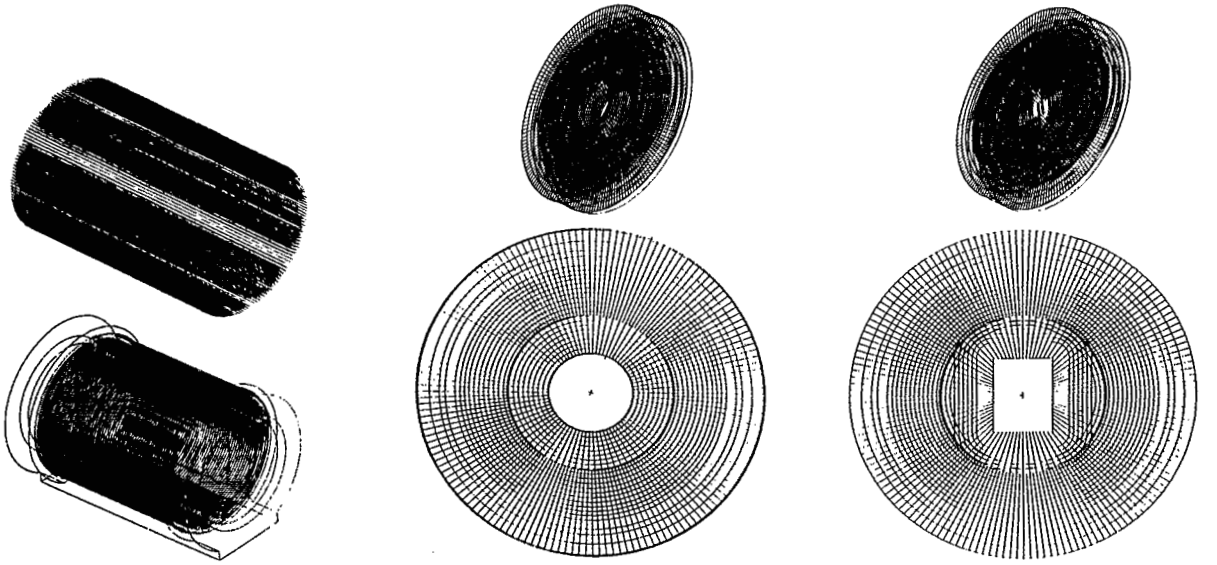

(a) Cylinder hoop and longitudinal rebar.

(b) Back wall hoop and radial rebar.

(c) Front wall hoop and radial rebar.

Figure 2. MTC primary rebar definition.

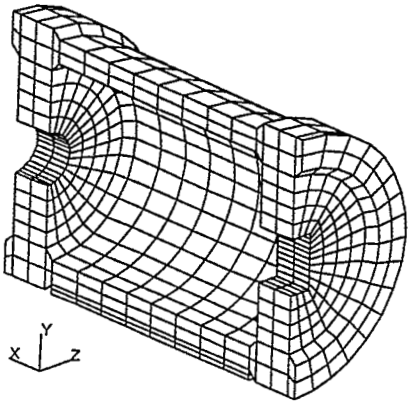

Figure 3. Three-dimensional finite element model for the MTC.

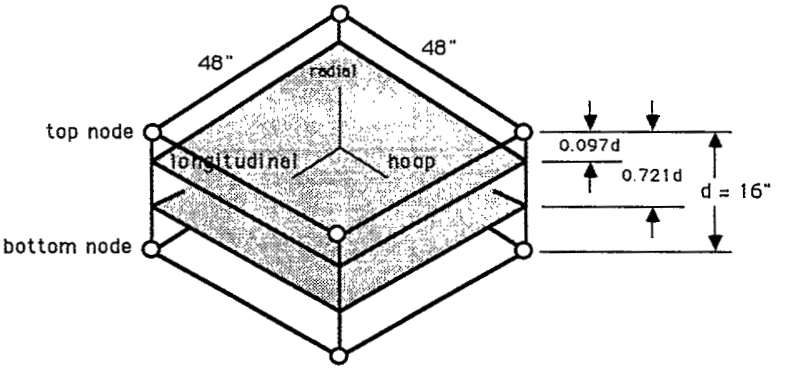

Figure 4. Typical embedded element for MTC model.

Embedded Reinforcement Element Test. Forces were applied to the nodes of a single embedded element (Figure 4) to demonstrate the anisotropy in load-deflection behavior due to the embedded steel reinforcement. The node forces were applied in the longitudinal, hoop and radial directions in separate tests. The applied nodal forces were uniform and predetermined such that without reinforcement, the plain concrete element would experience 1 psi axial stress in each case.

The numerical results of the three cases, with and without reinforcement present, are compiled in Table 1. The top and bottom node point displacements and element concrete stresses which were computed agree with the expected solution in the absence of the steel reinforcement. Comparison between these values and values computed with the reinforcement present demonstrated that the anticipated anisotropic behavior of the embedded reinforcement was present. The results showed that the steel reinforcement added more stiffness to the upper portion of the element in both the longitudinal and hoop directions, as would be expected from the placement of the two steel layers nearer the upper half of the element. Correspondingly, the element concrete stresses diminish below 1 psi in the longitudinal and hoop directions because the applied load is shared by the steel reinforcement. The element stiffness in the radial direction is otherwise insensitive to the longitudinal and hoop reinforcement.

Table 1. Embedded Element Behavior

Nodal Load Direction	Node Displacement (in. x 10^5)		Concrete Stress* (psi)	
	Without Steel Top/Bottom	With Steel Top/Bottom	Without Steel Top/Bottom	With Steel Top/Bottom
Longitudinal	1.600/1.600	1.261/1.317	1.000/1.000	0.800/0.810
Hoop	1.600/1.600	1.240/1.310	1.000/1.000	0.790/0.800
Radial	0.533/0.533	0.533/0.533	1.000/1.000	1.000/1.000

*Concrete stresses are reported at the top and bottom Gauss points.

MTC Reinforcement Model Description. ABAQUS provides a graphics package for visual checking of the input data specifying the location of embedded reinforcement. Samples of these graphics for the MTC model are shown in Figure 5, in which the reinforcement model is shown located relative to the three-dimensional finite element mesh. A longitudinal vertical section through the MTC's steel rebar cage model is shown in Figure 5a. For clarity, it is only one element deep in the direction perpendicular to the section. The four nested layers of longitudinal steel running horizontally through the cylinder wall and terminating at the end walls, are clearly visible at both the top and bottom of the cylinder. The thinner vertical lines uniformly spaced in the section of the cylinder wall represent stirrups.

Design of haunches in a conventional sense aims to provide fixity against rotation to develop the strength in adjoining walls and slabs. These graphics show how the crossing pair of diagonal bars in the haunch design of the MTC are modeled in detail. Each bar is modeled individually. This capability demonstrates unprecedented potential for accurately modeling the dynamic anisotropic interaction between walls and slabs in corner regions of explosive safety facilities in a reasonably automated fashion. Design and analysis procedures in explosive safety typically ignore this interaction which nonetheless is important to the overall dynamic response of magazines or missile test cells.

In Figure 5b, multiple layers of hoop and radial steel through the wall thickness are shown for the back wall. A similar model of the front wall reinforcement had an elliptical rather than a circular hoop reinforcement pattern near the aperature.

Nonlinear Concrete Material Model

The necessity of modeling nonlinear material behavior of concrete in explosive safety applications of finite element technology is apparent when it is considered that these structures are designed to sustain severe damage while containing or managing explosions. The anticipated extent of nonlinear material behavior might well vary with the particular facility, and modeling this behavior may be more important for some designs than for others. Compression behavior is important, for example, because compressive stresses equilibrate tension forces in steel rebar at cracked sections in flexure. Even if the compressive strength is not exceeded in such cases, the stress-strain behavior may well be nonlinear.

Moreover, failure of concrete in tension precipitates cracks which propagate and affect subsequent dynamic response. Nonlinear concrete material modeling is therefore primarily necessary for accurate determination of cracked surfaces and hence the structural modes which participate in the subsequent dynamic response of the structure.

Nonlinear concrete material models are generally very complex both theoretically and computationally. The overall complexity of modeling reinforced concrete is reduced somewhat by the strategy of modeling the reinforcement separately (e.g., using an appropriate reinforcement model) from modeling the concrete material behavior.

The interaction between reinforcement and concrete, known as bond-slip behavior, is rarely accounted for in today's technology. Bond-slip models are the subject of ongoing basic research at NCEL (Cox and Herrmann, 1992), as well as elsewhere. Such models have been used with embedded reinforcement models for steel, for example by Elwi and Hrudey (1989). However, the technique remains tentative and embryonic as the discussion by Pandey (1991) suggests. Schnobrich (1989) suggests that application of bond-slip models is currently prohibitive with large, nonlinear finite element analysis of reinforced concrete structures.

Theoretical Aspects. Theoretical complexity derives from the concepts of the theories of plasticity and continuum damage mechanics as applied to the failure of brittle materials. Such materials exhibit very different behavior for compression and tension loadings, and the material model is correspondingly very different for compression and tension stress-strain behavior. The ABAQUS concrete material model uses plasticity theory to describe crushing behavior and

damage mechanics for cracking behavior. These theories are combined to derive a constitutive, or stress-strain, law for overall material behavior. The constitutive law is ultimately expressed as a system of several nonlinear differential equations.

Computational Aspects. The constitutive law must be numerically integrated in a manner analogous to numerical integration of an initial value problem. Computational complexity derives from the algorithms used to integrate the system of equations along the stress-strain path at special points within each finite element known as stress points or Gauss points. For example, the nonlinear concrete material model implemented in ABAQUS, as described by Resende (1987, 1989), is over 4,000 lines of code in length. In an implicit nonlinear dynamic finite element analysis, this code sequence must be traversed for each Gauss point, within each element, for each iteration, within each load step, over the history of the dynamic response. For a single three-dimensional analysis using the MTC model, this could amount to over one million traverses of the material model loop. Clearly these analyses are not suited to personal computers, and require at least the use of very powerful workstations.

Practical Aspects. The ABAQUS nonlinear concrete model is limited to confining pressures below three to four times the concrete compressive strength. Hydrodynamic material models such as are available in DYNA3D offer an alternative in this regard when much higher pressures are encountered.

Furthermore, while the concrete material model handles severe loading, well beyond the elastic response, it is limited to relatively monotonic loads. The ABAQUS concrete material model should therefore be applicable to problems involving over pressurization of containment structures such as nuclear reactor containments or missile test cells since there is generally little interest in the response after only a very few cycles. Conversely, it is not suited to high performance magazine concepts wherein design pressures are of an order magnitude higher than the compressive strength, or to severe seismic loads where cyclic inelastic response with many cycles is important.

Nonlinear Dynamic Response of MTC Wall

It was discovered that the nonlinear dynamic response of the MTC using the aforementioned three-dimensional model could not be computed satisfactorily due to the extreme sensitivity to cracking of the concrete material model. In the material model, cracks form when the direct stress exceeds the tensile strength of concrete. Secondary cracks form in planes orthogonal to the plane containing the initial or primary crack. At most we were able to simulate only the first 1.6 ms of the dynamic response before secondary cracking took place, which could not be handled by the material model. This deficiency is now documented in ABAQUS version 4.9.

Simplified Model of the MTC Wall. To determine further the cause of the difficulty, a simpler model of the MTC wall was constructed. This model consisted of a transverse section through the cylinder, and was formed directly from a ring of solid elements from the center of

the three-dimensional model. Plain strain conditions were imposed on this layer of elements, so that the dynamic response derived from this model would be strictly applicable to the wall of an infinitely long tube possessing the cross-section shape of the MTC.

Attempts to run the simplified model were successful, but not before many failed attempts occurred which were similar to those for the three-dimensional model.

Post mortem data of failed runs indicated that primary radial cracks had formed in the wall in a rational manner, but that the directions of secondary cracks which also formed were arbitrary and meaningless. Furthermore, the occurrences of secondary cracks were correlated with occurrences of hashing in the reported hoop stress data in the MTC wall. The hashing, or occurrence of large spikes in the response, was spurious since subsequent to formation of radial cracks, the concrete hoop stress response should have diminished smoothly to zero with continued loading. It was found that boundary conditions at the base of the MTC induced high bending moment in the wall which caused severe cracking to occur, and this overburdened the concrete material model's capacity to handle cracking correctly. The difficulty was finally resolved when boundary conditions representing support at the base of the model were removed. Subsequent to that adjustment, the simplified model ran reasonably successfully.

Unfortunately, similar adjustment of the boundary conditions at the base of the three-dimensional MTC model did not noticeably improve subsequent simulation attempts. This model is more challenging to the concrete material model since the additional geometrical complexity induces severe stress concentrations, particularly at the interface between the cylinder and end walls, which leads to widespread cracking. These stress concentrations were clearly visible in the results of preliminary linear static runs with the three-dimensional model.

Dynamic Response of the MTC Wall. Using the unrestrained simplified model of the MTC wall, the nonlinear dynamic response was computed relative to the prescribed blast load (Figure 1). The simulation terminated after 30 ms. The displacement fields at three intermediate stages of the response are depicted in Figure 6 where the radial expansion of the wall and base are shown (exaggerated for clarity).

The nonlinear dynamic response at top dead center (TDC) of the wall is shown in Figure 7. The first peak occurred at 12 ms and the second peak occurred at about 28 ms as shown in Figure 7a. The second peak is slightly larger at 2.3 inches displacement on the cylinder inner radius.

The hoop stress response at TDC is shown in Figure 7b. These data are remarkable for they show the relationship between radial cracking of concrete and progressive transfer of hoop force to the steel reinforcement at this section. This information is important to a detailed understanding of how the MTC wall behaves in resisting load. It would otherwise be difficult to obtain this information experimentally in full scale or model field tests of any reinforced concrete structure or structural element subjected to severe blast loading. It typifies the potential contribution of modern computational structural dynamics methods in supplementing information gained from full scale or model tests in explosive safety research.

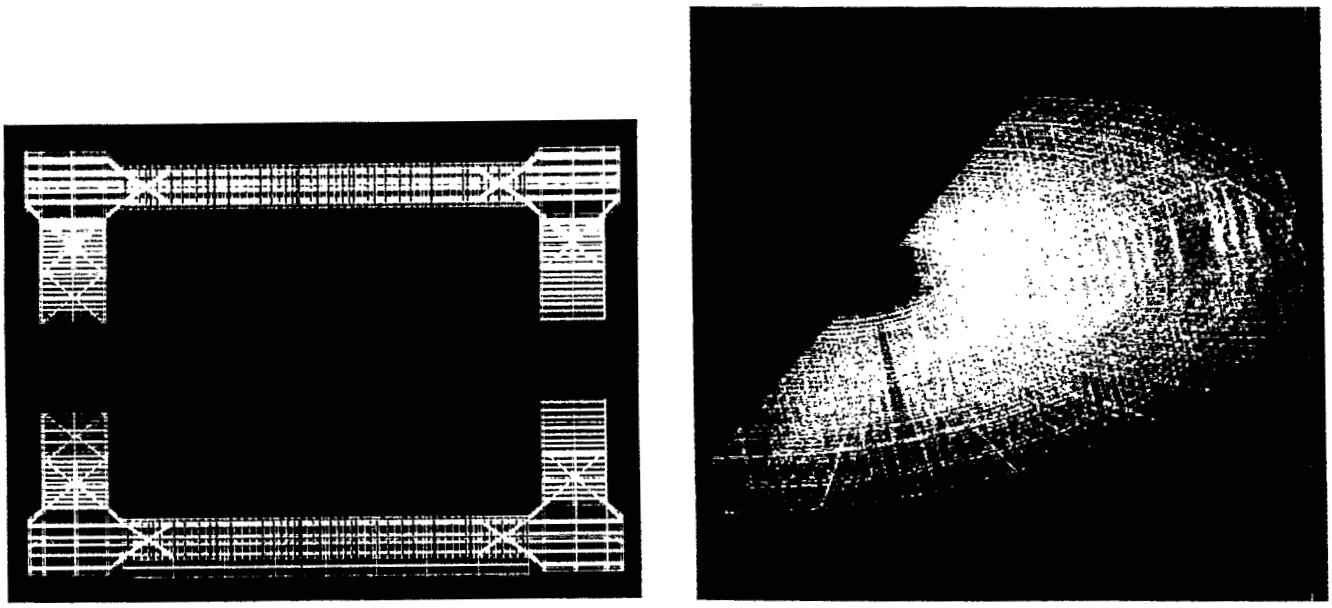

(a) Longitudinal section through cylinder.

(b) Isometric view of back wall model.

Figure 5. Embedded reinforcement model for MTC.

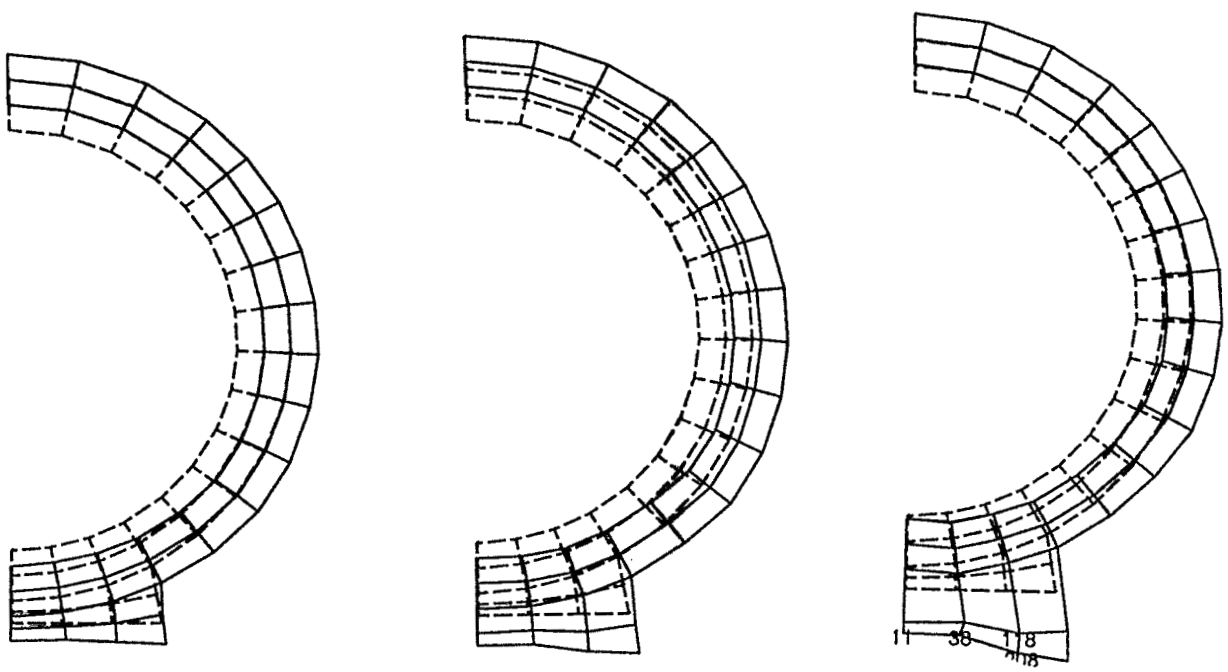

(a) t = 6.03 ms

(b) t = 12.00 ms

(c) t = 20.04 ms

Figure 6. Dynamic response of MTC wall.

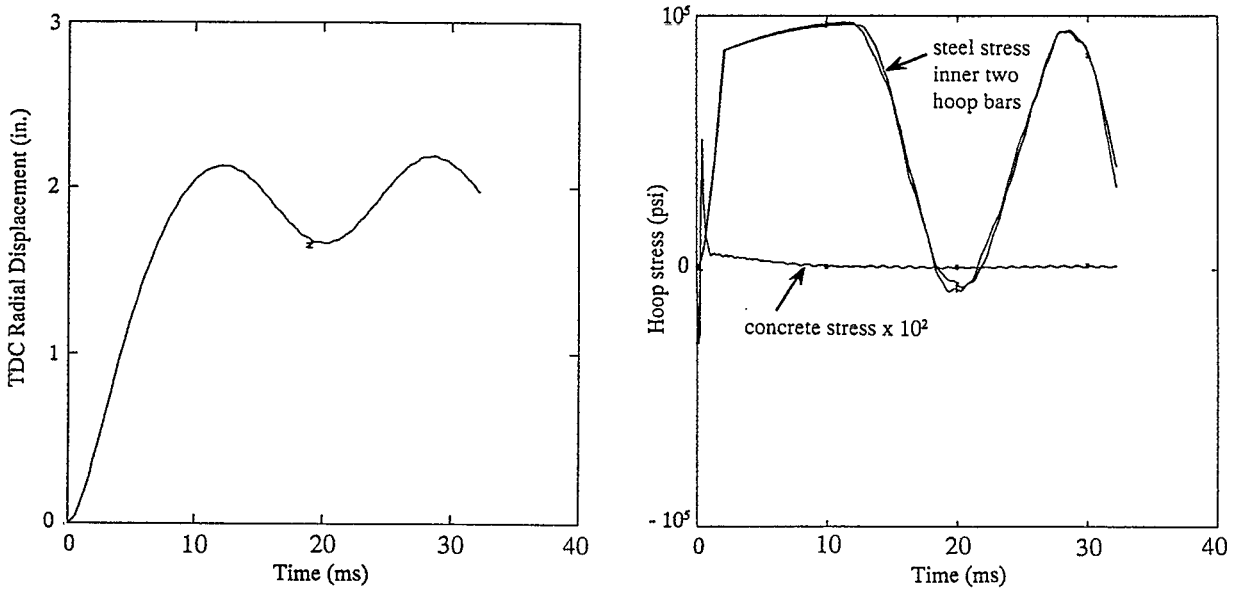

(a) Radial displacement response.

(b) Hoop stress response.

Figure 7. Dynamic response of MTC wall at TDC.

The aforementioned response results are from the inner finite element at TDC. Similar results also occurred for the outer element, thus indicating that the 32-inch wall was completely fractured at TDC. The peak tensile stress shown for the concrete is 540 psi, which was precisely the value prescribed in the material model for the tensile strength of concrete. The section completely cracks within the first millisecond, and data from other finite elements in the wall indicate that this response was also typical of most of the wall. That is, the concrete strength of the wall was not a factor after the first millisecond in resisting the residual gas pressure impinging on the wall.

The hoop steel reinforcement was seen to carry the load for the great majority of the dynamic response. These results tend to corroborate the assumption made in the MTC design that the concrete strength plays a negligible role in resisting internal blast loads and may be ignored (Ayvazyan et al., 1988).

The two inner layers of hoop reinforcing bars are shown to yield at the prescribed value of 86.7 ksi (Ayvazyan et al., 1988) within the first three milliseconds. Again these data were typical of the entire section and of most of the wall. Prescribed strain hardening of the bars was also evident in the response subsequent to yield until such time as the wall rebounded after 12 milliseconds had elapsed. Complete unloading of the hoop reinforcement was indicated, and in fact the bars momentarily experience compression before the second cycle of the response. These data warn that buckling of reinforcing bars designed primarily to resist tension forces is often a possibility due to rebound. A similar observation is made in the subsequent description of the computed dynamic response of reinforced concrete slabs.

NONLINEAR DYNAMIC FINITE ELEMENT ANALYSIS OF REINFORCED CONCRETE SLABS

An assessment of explicit finite element methods using the program DYNA3D is carried out in this section. Data from blast tests of reinforced concrete slabs conducted by NCEL were used to evaluate the calculations of dynamic response from DYNA3D as well as from standard NAVFAC P-397 single-degree-of-freedom (SDOF) methods. It is shown that finite element technology can provide very detailed insight into the structural response as well as improved accuracy for close-in blast loads.

Slab Test Program Overview

Dynamic blast load tests have been conducted on 12 two-way reinforced concrete slabs to verify shear reinforcement design criteria for NAVFAC P-397. Test results were reported by Tancreto (1988).

The test setup is shown in Figure 8. A 7.5 x 7.5 x 8 ft. deep cubicle was used to support the test slabs. The 10.5 x 10.5 ft. slabs (clear span 7.5 ft) had their outer 1.5 ft. edge clamped to the cubicle top.

Only slabs I and V were analyzed in the present study. Slab I had 1.06% (each way, each face) longitudinal steel (#2 deformed bars, yield stress 74.5 ksi) at d/2 spacing, W1 stirrups (yield stress 60 ksi) at d/2 spacing, a 4.5-in. thickness, and an effective depth d = 3.1 in. Slab V was designed with no shear steel, had a longitudinal steel percentage of 0.31% with #2 bars at d spacing, a 6-in. thickness and a 4-in. effective depth.

Spherical Composition C4 explosives (60 lbs) were used to generate the blast loads (TNT equivalency by weight of 1.13). Scaled standoff distances were 0.69 and 1.1 ft/lb$^{1/3}$ for slabs I and V, respectively.

Finite Element Models of Slabs

A three-dimensional nonlinear dynamic analysis of the two slabs was carried out using DYNA3D. In the finite element model, eight node solid elements and two node truss elements were used to represent the concrete slabs and steel bars, respectively. Representation of bars directly using truss elements is known as a discrete reinforcement model. Due to double symmetry, only 1/4 of the slabs was discretized as shown in Figure 9. The solid elements are 3x3 inches in plan with variable thickness. Four elements are used through the depth. Truss elements are located on the first layer in from each face. The steel area was lumped at 3 inches on center as dictated by the size selected for the solid elements.

To facilitiate comparison to SDOF models the load was first assumed to be uniformly distributed. The corresponding idealized triangular load history decreased from 5,724 to 0 psi in 0.2 ms for slab I, and from 3,564 to 0 psi in 0.264 ms for slab V. A second round of analyses considered a non-uniform load distribution. Pressure load histories were obtained using the program SHOCK (NCEL 1988) in the absense of measured blast load data.

To verify the different material models available in DYNA3D for the behavior of concrete and steel, single elements were analyzed under tension and compression loads. From these tests, material models 3 and 16 were chosen as best suited for steel and concrete, respectively.

Concrete properties used were as follows: the modulus of elasticity was 4,000 ksi, Poisson's ratio was 0.2, and the dynamic compressive strength was 6,000 psi. A dynamic increase factor DIF of 1.25 to account for strain rate effects on strength was specified from NAVFAC P-397. The pressure versus volumetric strain graph for specifying the equation of state in DYNA3D material model 16 was used for concrete. For steel, the modulus of eleasticity was 29,000 ksi, the Poisson ratic was 0.3, the dynamic yield stress was 97 ksi (DIF 1.3), and the dynamic ultimate stress was 102 ksi (DIF 1.05).

Results and Discussion of the Dynamic Response for the Slabs

DYNA3D computations of the dynamic response, as well as design values from standard NAVFAC P-397 single-degree-of-freedom (SDOF) methods, are compared to limited experimental test data in the following.

Experimental Results. Measured maximum residual deflections were 8 and 8.3 inches at the center of slabs I and V, respectively. These deflections were measured after rebound, and are less than the maximum deflections reached during the tests. The deformed shapes, including yield line formations, were also apparent in Figure 10. For slab I, classical yield lines formed along the diagonals (Figure 10a). Slab V however exhibited a circular yield line about 9 inches from the sides (Figure 10b). During the rebound phase buckling of the lower reinforcement at the center of both slabs was observed.

SDOF Predictions. Design deflections, which included membrane action, were found using SDOF modeling procedures from NAVFAC P-397 using the computer program SOLVER (Holland, 1989). The results were 5.5 and 6.1 inches for the centers of slabs I and V, respectively.

Using the simplified procedure in NAVFAC P-397, employing a constant plastic resistance function, and design values for both steel and concrete, maximum deflections were calculated again yielding 6.8 and 6.9 inches for slabs I and V, respectively. These values are closer to measured residual values and represent an upper bound for SDOF predictions. Figure 11 shows the dynamic response data for the slabs.

In all cases, SDOF calculations of maximum response were less than the measured residual deflections. Although maximum predictions are only 15% off, they are unconservative. This could be due to the fact that the SDOF model was employed assuming an equivalent uniform load distribution which is not as severe as assuming a non-uniform load distribution.

DYNA3D Predictions. Figure 11 also shows the dynamic response of both slabs using DYNA3D. Experimental residual deflections fall between the residual deflection values predicted by the uniform and non-uniform load cases, the former being unconservative and the latter being conservative.

Computed displacement fields at specific times are shown in Figure 12. Figure 12a shows the deformed shape of slab I at peak displacement under uniform and non-uniform loads. Classical yield lines for this slab are indicated by the greater deflections along the diagonals. Figure 12b shows the deformed shape of slab V at 50 ms (displacements enhanced for clarity). Experimental yield line patterns for slab V were circular, and the finite element model also computed a circular localized deformation for this case.

Figure 13 shows a typical stress-time history of a bar located at center bottom of slab V. Initially, both top and bottom steel bars go into compression (less than 16 ksi for all cases) for a very short time while the shock load is still being applied. Later both top and bottom steel go into tension reaching yield stress, indicating that membrane action is taking place. During rebound, top and bottom bars unload and go into relatively high compression. In practice, these high compression stresses will not be reached because the bars are usually not braced against buckling. Buckling of the lower bars was discovered in photographs of the tested slabs as a result of analysis of these finite element data. However, beyond the indication of potential buckling in bars the finite element simulation was not necessarily accurate because it did not account for buckling phenomena.

Summary of Alternative Methods. In the case of close-in explosions it appears from these results that SDOF design criteria predictions can be unconservative unless the non-uniformity of the load is some how accounted for when computing the dynamic response. DYNA3D predictions with uniform and non-uniform loading, using material model 16, provided lower and upper bounds for the measured residual deflections. Dynamic responses from DYNA3D with uniform loading assumed were in reasonably close agreement with results from SDOF models. In addition, the finite element models provided an efficient and accurate way to obtain detailed information on the nonlinear dynamic response and structural behavior of flat slabs, including yield line pattern, concrete and rebar stress histories, and prediction of the potential for reinforcement buckling.

NONLINEAR DYNAMIC FINITE ELEMENT ANALYSIS OF A SOIL-COVERED REINFORCED CONCRETE ROOF

The explicit finite element code DYNA3D was evaluated for a problem involving much higher blast loading pressures. A soil-covered reinforced concrete slab represents the roof of a proposed high performance magazine concept, currently being developed at NCEL, consisting of several adjacent cells for efficient explosives storage.

The objective of the numerical analysis is to determine the dynamic behavior of the roof slab due to a very high pressure (up to 24 ksi) explosion in one of the cells. This study also included examination of computed initial debris velocities of concrete fragments emanating from the failed slab.

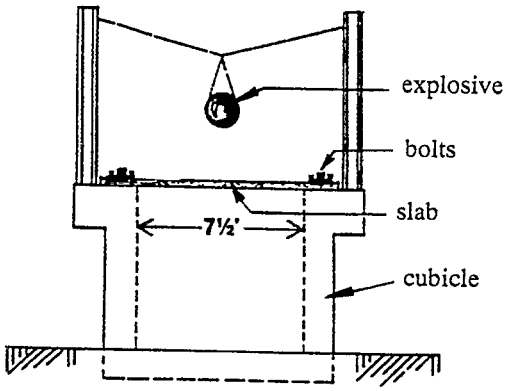

Figure 8. Slab test set-up.

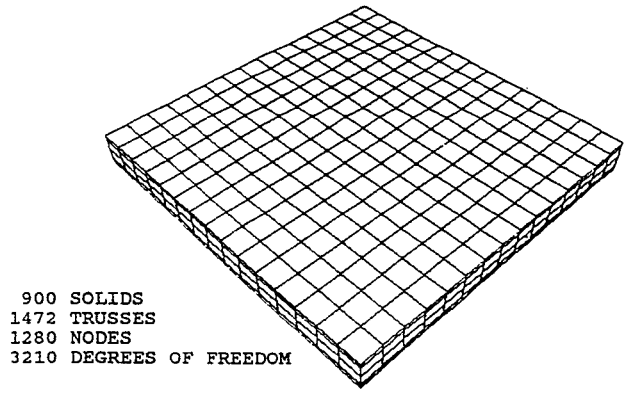

Figure 9. Finite element mesh.

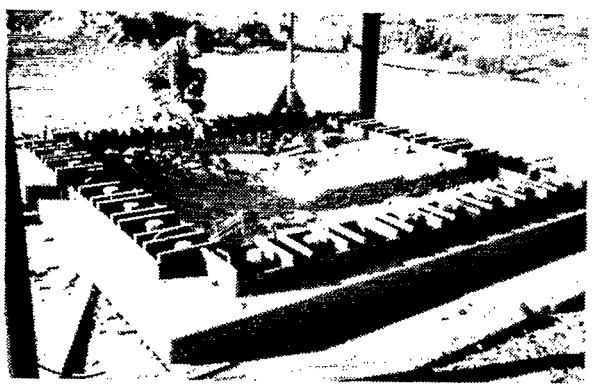

(a) Slab I

(b) Slab V

Figure 10. Top view of slabs after failure.

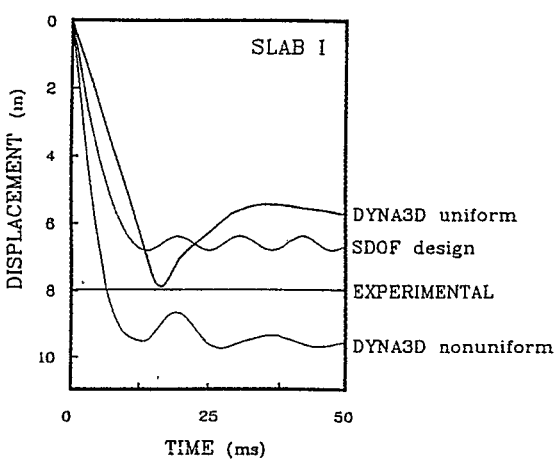

(a) Slab I

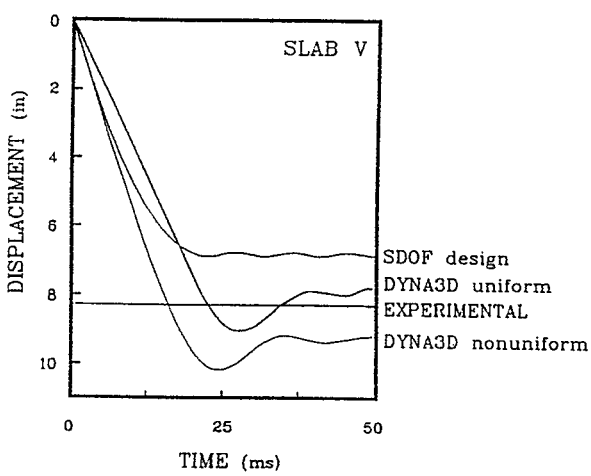

(b) Slab V

Figure 11. Dynamic response, center of slabs.

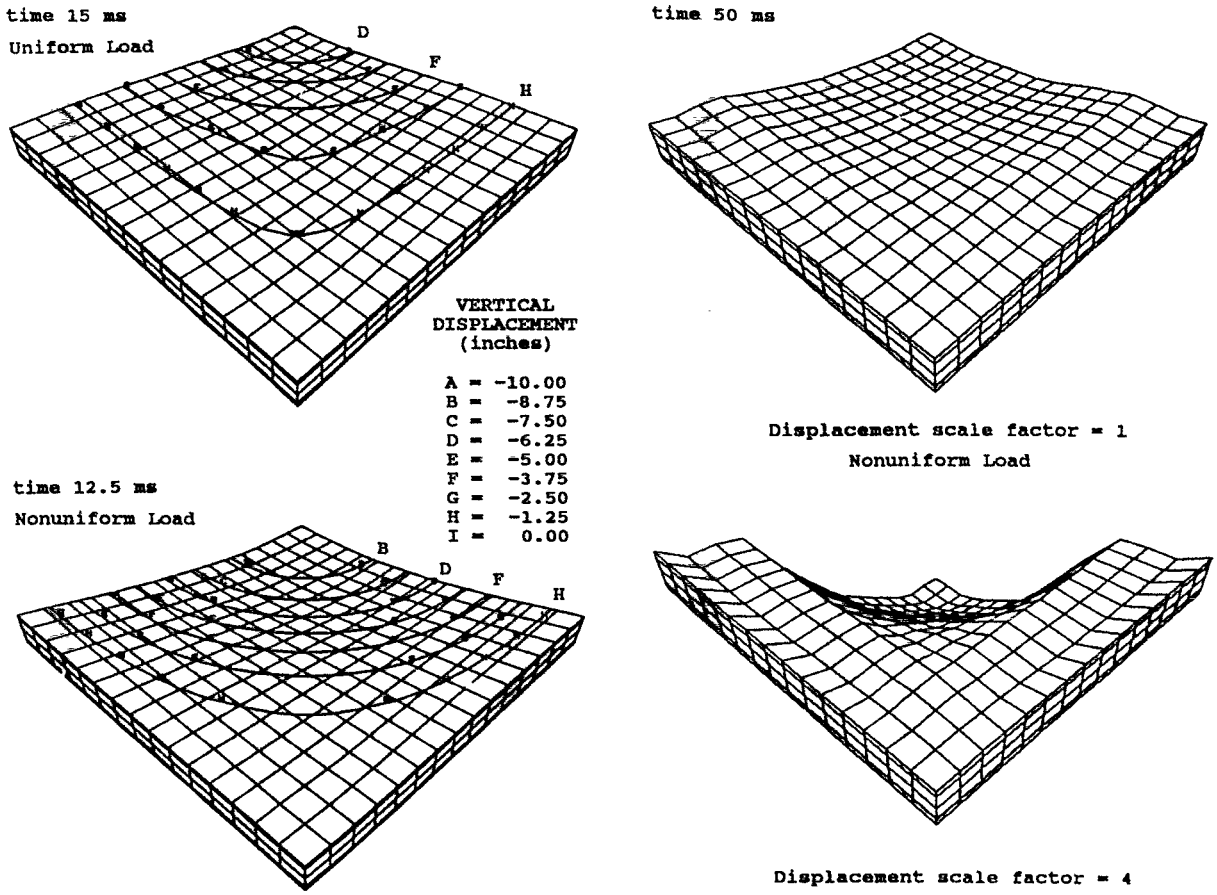

(a) Slab I, peak displacement

(b) Slab V

Figure 12. Deformed shapes.

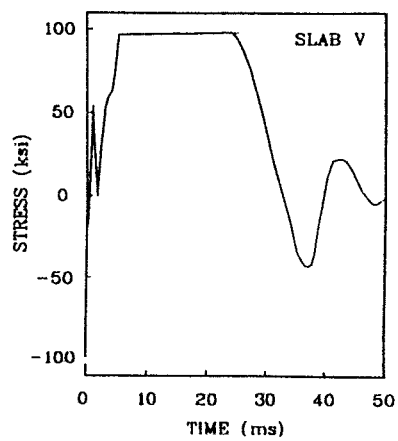

Figure 13. Rebar stress history; center, bottom bar non-uniform load.

Reinforced Concrete Roof

The high performance magazine is designed to store a large amount of munitions in a small area, thus reducing the encumbered land around storage facilities required for safety. The preliminary design for the magazine is that of a large buried structure with munitions to be stored in cells, as shown in Figure 14.

The roof is a 2-foot thick reinforced concrete slab constructed of 4,000-psi concrete (150 lb/ft^3) with top and bottom reinforcement of Grade 60, #9 bars running in both directions at 10 inches on center. Shear reinforcement consisting of Grade 60, #4 bars connects each intersection of the longitudinal bars across the top and bottom of the slab.

The roof primarily functions as a one-way, simply supported plate carrying four feet of soil cover (110 lb/ft^3). The soil cover provides mass for enhancing kinetic energy dissipation of the blast energy. Since the soil cover is presumed to be unreinforced, no resistance is expected from its strength (only its inertia will contribute). The roof is supported by the outer walls and the middle wall in the long direction. It is lightly connected to these walls, and this connection is designed to offer no resistance to uplift due to an internal explosion.

The wall design of the cells is aimed at preventing sympathetic detonation, so that an explosion in one cell will not detonate munitions stored in another cell. The roof, however, will be subjected to the full force of the explosion and is designed to suffer considerable damage and absorb most of the energy released (through strain energy mechanisms involving nonlinear material behavior and large residual deflections). Due to the cell concept, the blast load will be off center and nonuniform, as shown in Figure 15a.

Blast loads were obtained using the program SHOCK, as described in the previous study. A charge of 10,000 lbs detonated in a central cell was simulated. Figure 15a shows the shock wave scaled impulse loading (units are $psi\text{-}ms/lb^{1/3}$). Pressure values are obtained from $P = 2I/t$, where I = scaled impulse x 24.27 (scaling factor, $lb^{1/3}$) and $t = 4.06$ ms is the load duration, which is assumed constant over the roof. The load time history at a point above the charge is shown in Figure 15b. It includes both the initial shock load and the residual gas pressure. The gas pressure load is relatively low but lasts for 20 seconds.

Finite Element Model of the Roof Slab

The concrete slab was represented via eight-node three-dimensional solid elements. Two solid elements were used through the depth. To simplify the discretization, the concrete cover was not modeled but its mass was added to the concrete core. Element generation was carried out using the DYNA3D preprocessor program INGRID (Stillman and Hallquist, 1985), as well as a custom made preprocessor. A top view of the finite element mesh is shown in Figure 16. The single plane of symmetry for the problem is exploited.

To accurately capture the response of the reinforcement, a discrete reinforcement model of the steel in the roof was implemented. This method is generally more accurate than a smeared or an embedded reinforcement model, and well suited for reinforcement patterns which are regular. Although an embedded model would also be efficient, it is not available in DYNA3D.

Top and bottom steel meshes were modeled using discrete two-node truss elements located at 20 inches on center, i.e. each element representing the contribution of 2 bars. Similarly, the shear reinforcement was lumped at 20 inches on center, each truss modeling the cross sectional area of 4 bars lumped together. The way in which the steel bars are lumped together depends on the design of the three-dimensional discretization of the concrete slab.

Material Models and Properties

An evaluation of the material models available in DYNA3D was performed to find suitable models for the reinforcing steel and the concrete. The evaluation consisted of compressive and tensile tests on single truss and solid elements in the expected stress and strain ranges. For steel, material model 3, an elastic-plastic model with isotropic/kinematic hardening, exhibited the expected elastic plastic behavior. For concrete, linear and nonlinear responses with materials models 17, 16, 5 and 25 were evaluated using an 8-node solid element. Material model 16, a concrete/geological material model, with no smeared reinforcement was determined most suitable for plain concrete. In tension, it accurately captured cracking of the concrete, whereas in confined compression it was able to reproduce the behavior of concrete under pressures in excess of the 24 ksi peak pressure. This peak pressure is four times higher than the compressive strength of concrete and could not be handled by the ABAQUS material model for concrete according to Resende (1989). The direct use of ABAQUS is precluded for this problem not only because it is an implicit code, but also because of acknowledged material model restrictions.

Concrete and reinforcement were modeled with the properties shown in Table 2. The program internally generates the remaining concrete properties. Yield stress and compressive strength were increased to account for strengthening due to high strain rates.

Table 2. Material Properties for the DYNA3D Roof Slab Model

Steel:	Young's modulus	E = 29,000,000 ksi
	Poisson's ratio	μ = 0.3
	Yield stress	σ_o = 82.5 ksi (DIF 1.25)
	Tangent modulus	E_t = 447 ksi
	Hardening Parameter	β = 1
Concrete	Poisson's ratio	μ = 0.2
	Compressive strength	f_c' = 6000 psi (DIF 1.25)
	Cohesion	a_o = -1

Dynamic Response of Soil-Covered Roof Slab

The deformed shape of the roof slab (enhanced five times) is shown in Figure 17 at two different time steps in the dynamic response. It is observed that the displacement field is very localized. However, there is also a rigid body displacement component in the long-term computed dynamic response. For example, the entire roof rises uniformly about 8 inches in 30 ms.

Figure 18 shows the concrete stresses in the plane of the slab. Upon arrival of the shock wave the concrete goes temporarily into compression, then unloads, cracks in tension and loses all load-carrying capacity. The elements closest to the load are subjected to longer lasting and more severe compression, as should be expected due to local slab bending. After element cracking, the concrete mass is assumed to be still acting on the system. However, cracking of the top elements occurs at 2.5 milliseconds and it is expected that the concrete cover would then separate from the roof slab and generate debris.

Figure 19 shows the stresses in ten lower reinforcing bars along the plane of symmetry, five on each side of the point of maximum load. Some of the bars are seen to reach yield between 16 and 18 ms. At that point it is expected that additional debris will separate from the roof slab.

Figure 20 shows contours of the velocity field at 7 ms and at 27 ms. The velocity time history at the point just above the load yields the highest velocity, 2500 in/sec, which is reached at about 8.5 ms, as shown in Figure 21. Knowledge of the velocity field at various times facilitates computing the distance of debris fallout, which in turn will help characterize the effectiveness of the soil-covered roof slab concept.

Calculations for the dynamic response of the high performance magazine indicated that blast effects on the roof will be highly localized. The concrete directly above the blast should crush early, then carry pressure hydrodynamically during the shock load phase.

Debris Prediction Data. Calculations of the dynamic response also indicated that the rebar directly above the blast load will yield and snap early, thus reducing the concrete confinement and releasing parts of the roof slab as debris. The model did not allow for direct prediction of actual debris and release of broken bars, and the predicted dynamic response will therefore diverge from the actual one when the reinforcing bars reach their ultimate capacity. However, debris distance predictions can be facilitated with this data as follows:

(1) knowledge of the complete concrete stress field and rebar stress response as a function of time allows the determination of the time and the amount of debris separation;

(2) knowledge of the complete velocity field as a function of time allows the determination of initial debris velocities;

Similar calculations of debris velocity from slabs using DYNA3D have been reported (Terrier and Boisseau, 1989) where agreement is shown with debris velocity measurements.

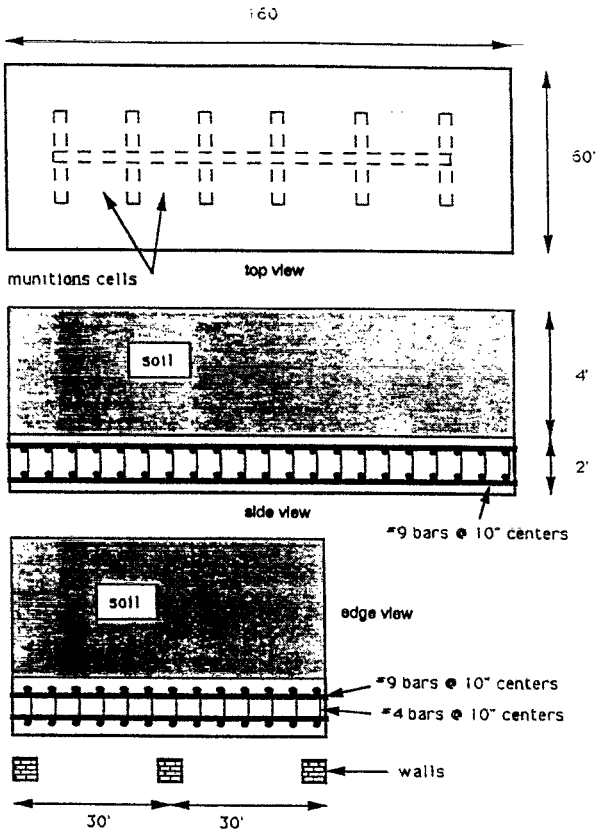

Figure 14. Preliminary high performance magazine roof design.

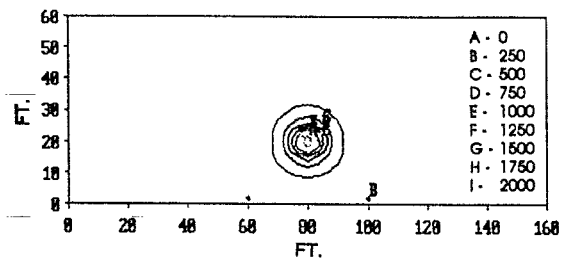

(a) Scaled shock impulse distribution

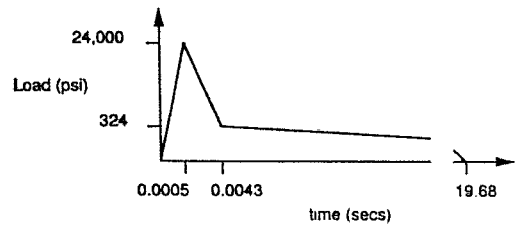

(b) Load time history (values at max. pt.)

Figure 15. Design roof slab load.

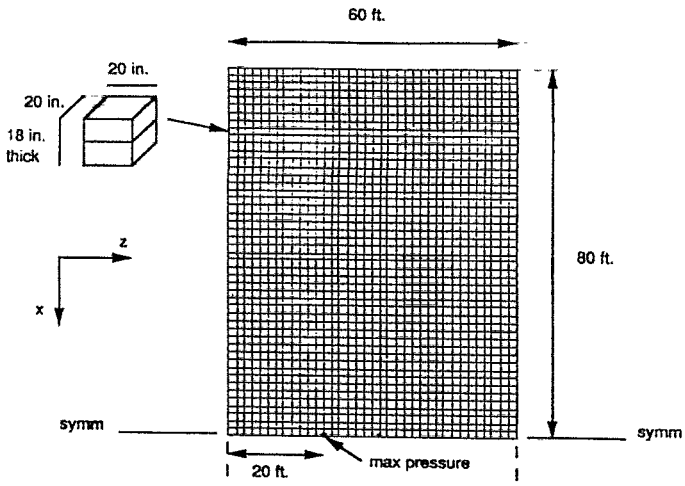

Figure 16. Finite element mesh.

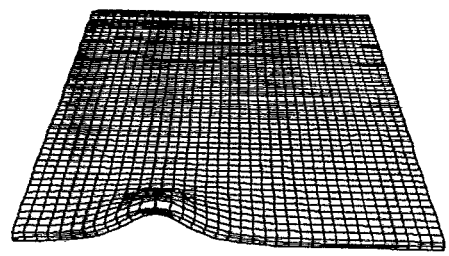

(a) At 7 ms

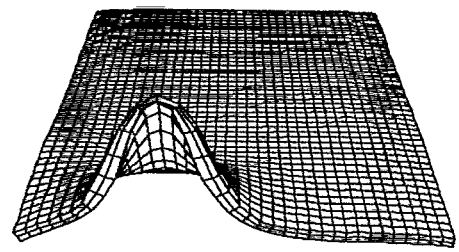

(b) At 27 ms

Figure 17. Deformed shape (enhanced 5 times).

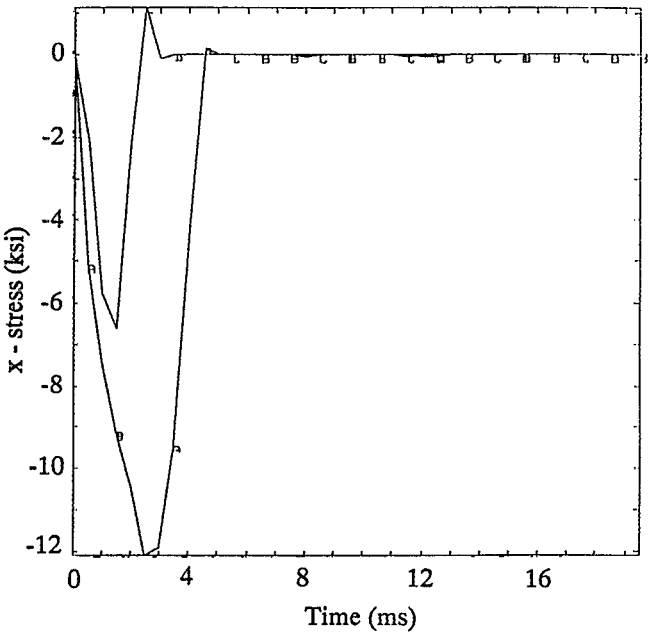

Figure 18. Horizontal stresses in concrete.

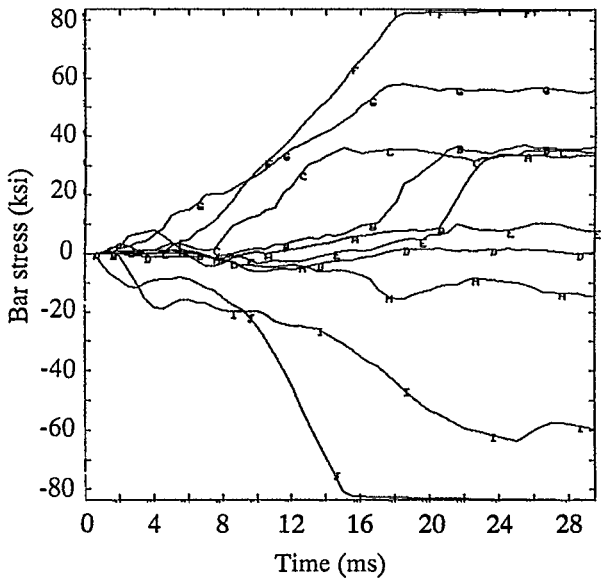

Figure 19. Reinforcing bar stresses.

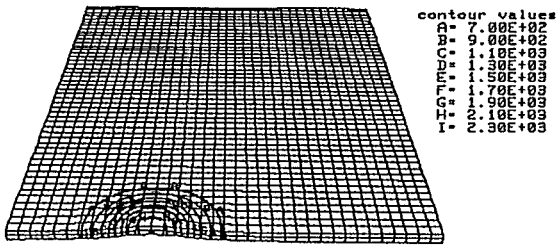

(a) At 7 ms

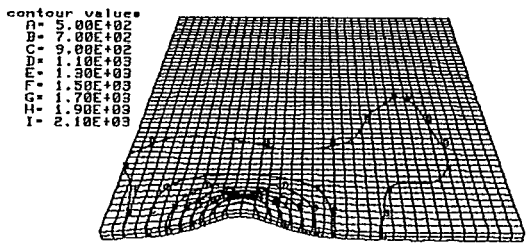

(b) At 27 ms

20. Vertical velocity contours (in/sec).

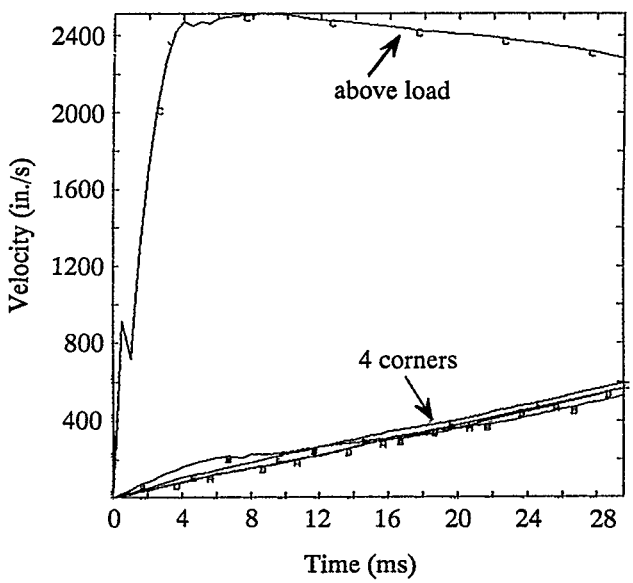

Figure 21. Vertical velocity histories.

Independent calculations using the program FRANG (Wager and Connet, 1989) determined the average velocity of debris from a 16- by 28-foot breached area directly above the cell. The program calculates pressure time histories resulting from an explosion in a room which has vents and frangible panels, i.e. panels designed to break loose and provide additional vent area. Displacement, velocity and acceleration histories of the frangible panels are also determined.

It was found that for the weight of a 4-foot soil cover, the average maximum velocity of the debris would be 2400 in/sec (Murtha, 1992). Those calculations assume that fragments have already separated from the roof, and their velocities were therefore expected to be somewhat higher than velocities calculated by DYNA3D. From Figures 20 and 21 it is observed that the velocity field above the cell at 8.5 ms (maximum values) varies between 700 and 2500 in/sec for an area of about 20 by 20 ft.

Recent NCEL field tests on a 1/10 scale model of a high performance magazine (Murtha, 1992) have qualitatively confirmed localization of the deformations and breaching of the roof above the cell which had been predicted by the results from the three-dimensional nonlinear dynamic finite element analysis.

Summary of Soil-Covered Roof Slab. The explicit finite element program DYNA3D was successfully used in modeling the soil-covered roof slab which was subjected to an unusually severe blast load. It was shown that concrete and reinforcing bar stress histories can be obtained, yielding information on cracking, concrete cover separation, bar yielding and rupture. Initial debris velocity fields can also be determined, which in turn facilitate the calculation of debris distances.

CONCLUSIONS

Three-dimensional nonlinear dynamic finite element studies have been carried out for three classic problems in Navy explosive safety engineering; these include a specialized missile test cell design concept, reinforced concrete slabs with variable shear steel design, and a soil-covered roof design for a proposed high performance magazine. Two widely available general purpose computer programs were applied in these analyses, one based on implicit and the other based on explicit temporal integration of the equations of motion.

Application of these computer programs can provide a viable alternative to codified single-degree-of-freedom (SDOD) methods currently used in the design and analysis of explosive safety structures. This modern technology can be at least as accurate as historical SDOF methods for computing dynamic response, and can provide substantially more detail on structural behavior, particularly when special structural concepts are encountered.

Concrete material models which have been implemented in commercial implicit computer programs are sophisticated, but they can be unreliable and cause simulations to terminate prematurely. This difficulty is partially offset in programs that provide for users to supply their own specialized material model subroutines which may be more suited to specialized problems. Implicit programs were found to provide for excellent reinforcement modeling capability when

they supported embedded reinforcement modeling. This capability is important for explosive safety because many designs include heavily reinforced sections and complicated reinforcement patterns in both two- and three-dimensional configurations.

Explicit programs are more robust regarding large-scale numerical solutions of highly nonlinear equations of motion describing the dynamic response of explosive safety structures. However, their concrete material models are less mature than corresponding material models in implicit programs. Moreover, reinforcement modeling is not as well supported in explicit programs. Although they can model regular patterns of reinforcement, often found in slab designs for example, they cannot model more complex patterns efficiently without embedded modeling capability.

In summary, general purpose computer programs for three-dimensional nonlinear dynamic finite element analysis represent a powerful tool for specialized problems in explosive safety, as well as an attractive alternative for codified SDOF methods. Accurate models of specialized reinforced concrete missile test cells and magazines can be constructed more fficiently using available implicit programs, whereas, available explicit programs yield successful simulations with less difficulty.

ACKNOWLEDGMENTS

The Computer Aided Design Division, Code 1082, NWTC, Point Mugu, supplied the Sun Workstation used in the MTC study; Doug Doi and Jim Thompson were instrumental in the MTC modeling work. At HKS (West), Inc., Nuno Rebelo and Tod Dalrymple provided valuable user support in the application of ABAQUS. Robert Whirley at Lawrence Livermore National Laboratory kindly supplied DYNA3D tapes and documentation to NCEL. At NCEL, Bob Murtha and Jim Tancreto provided useful discussions on aspects of explosive safety design and field test results.

REFERENCES

ABAQUS User's Manual, Version 4.8, Hibbitt, Karlsson and Sorensen, Inc., 100 Medway St., Providence, RI 02906, 1989 (1080 Main St., Pawtucket, RI 02860).

Army TM 5-1300 / Navy NAVFAC P-397 / Air Force AFR 88-22 (1991). Structures to Resist the Effects of Accidental Explosions. Washington, DC.

Ayvazyan, H.E., M. Dede and N. Dobbs (1988). "Design of NAVFAC Type VB Missile Test Cell," Ammann & Whitney Consulting Engineers, New York, NY, Aug 1988.

Biggs, J.M. (1964). Introduction to Structural Dynamics, McGraw-Hill Book Co., New York, NY, 1964.

Cervera, Hinton and Hassan (1987). "Nonlinear Analysis of Reinforced Concrete Plate and Shell Structures Using 20-Noded Isoparametric Brick Elements." Computers and Structures, Vol. 25, No. 6, pp 845-869, 1987.

Cox, J.V., and L.R. Herrmann (1992). "A Plasticity Model for the Bond Between Matrix and Reinforcement," 6th Japan-U.S. Conference on Composite Materials, Orlando, FL, 22-24 Jun 1992.

Elwi, A.F., and T.M. Hrudey (1989). "Finite Element Model for Curved Embedded Reinforcement," ASCE J. of Engr. Mech., Vol. 115, No. 4, 1986. Discussion by P.C. Pandey, Vol 117, No. 3, pp 714-715, Mar 1991.

Hallquist, J.O., and R.G. Whirley (1989). DYNA3D User's Manual, UCID-19592, Rev. 5, Lawrence Livermore National Laboratory, P.O. Box 808, Livermore, CA 94550, May 1989.

Holland, T.J. (1989). SOLVER User's Guide, Version 2.2, Dynamic Response Analysis of SDOF Systems, CAE Structures Library UG-0020, Naval Civil Engineering Laboratory, Port Hueneme, CA 93043.

Murtha, R.N. and M. Dede (1988). Internal Working Memorandum: "Test Plan for Explosives Safety Certification of NAVFAC Standard Type V Missile Test Cell." Naval Civil Engineering Laboratory, Port Hueneme, CA 93043, Dec 1988.

Murtha, R. (1992). Small-scale High Performance Magazine Roof and Soil Cover Tests. Personal communication, Naval Civil Engineering Laboratory, Port Hueneme, CA 93043.

PATRAN Plus User Manual, Release 2.4, PDA Engineering, 2975 Redhill Ave., Costa Mesa, CA 92626, Sep 1989.

Resende, L. (1987). "A Damage Mechanics Constitutive Theory for the Inelastic Behavior of Concrete," Computer Methods in Applied Mechanics and Engineering, Vol. 60, pp 57-93, 1987.

Resende, L. (1989). Personal communication, ABAQUS Training Course, Providence, RI, Oct 1989.

Schnobrich, W.C. (1989). "Reinforced Concrete Shells: Some Problems," Analytical and Computational Models of Shells, Eds. Noor, Belytschko and Simo, CED-Vol. 3, ASME, 1989.

Shugar, T.A., T.J. Holland, and L.J. Malvar (1992). "Three-Dimensional Finite Element Analysis of Explosive Safety Facilities - A Technology Assessment," Naval Civil Engineering Laboratory, Port Hueneme, CA 93043 (in publication).

Stillman, D.W. and Hallquist, J.O. (1985). INGRID: A three-dimensional mesh generator for modeling nonlinear systems, Lawrence Livermore National Laboratory, CA.

Tancreto, J.E., and E.S. Helseth (1984). "Effect of Frangible Panels on Internal Gas Pressures," Minutes of the Twenty-First Explosives Safety Seminar, Department of Defense Explosives Safety Board, Aug 1984.

Tancreto, J.E. (1988). "Dynamic Tests of Reinforced Concrete Slabs," Proceedings, 23rd Department of Defense Explosives Safety Board Seminar, Atlanta, GA.

Terrier, J.M., and J.F.K. Boisseau (1989). "Numerical Simulation of Reinforced Structure Response Subjected to High Explosive Detonation," Proceedings of the Fourth International Symposium on the Interaction of Non-nuclear Munitions with Structures, Vol. 1, Panama City Beach, FL, Apr 17-21, 1989.

Wager, P. and Connet, J. (1989). FRANG Users's Manual, Naval Civil Engineering Laboratory, Port Hueneme, CA 93043.